Aggregation state and magnetic properties of magnetite nanoparticles controlled by an optimized silica coating

Nicolás Pérez, C. Moya, P. Tartaj, A. Labarta, and X. Batlle

Articles you may be interested in

Static and dynamic magnetic properties of spherical magnetite nanoparticles
Journal of Applied Physics **94**, 3520 (2003); 10.1063/1.1599959

Fundamentals and advances in magnetic hyperthermia
Applied Physics Reviews **2**, 041302 (2015); 10.1063/1.4935688

Simple models for dynamic hysteresis loop calculations of magnetic single-domain nanoparticles: Application to magnetic hyperthermia optimization
Journal of Applied Physics **109**, 083921 (2011); 10.1063/1.3551582

Thermal transport at the nanoscale: A Fourier's law vs. phonon Boltzmann equation study
Journal of Applied Physics **121**, 044302 (2017); 10.1063/1.4974872

Effect of magnetic dipolar interactions on temperature dependent magnetic hyperthermia in ferrofluids
Journal of Applied Physics **121**, 023901 (2017); 10.1063/1.4973879

Synthesized $MoSe_2/TiO_2$ heterogeneous structure as the promising photocatalytic material: Studies from theory to experiment
Journal of Applied Physics **121**, 044303 (2017); 10.1063/1.4974911
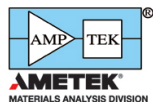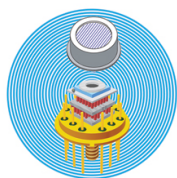
Aggregation state and magnetic properties of magnetite nanoparticles controlled by an optimized silica coating

Nicolás Pérez,[1,2,a)] C. Moya,[2,3,a),b)] P. Tartaj,[4,a)] A. Labarta,[2,a)] and X. Batlle[2,a)]

[1]*Institute for Metallic Materials, IFW-Dresden, Helmholtzstrasse 20, 01069 Dresden, Germany*
[2]*Departament de Física de la Matèria Condensada and Institut de Nanociència i Nanotecnologia (IN2UB), Universitat de Barcelona, Martí i Franqués 1, 08028 Barcelona, Spain*
[3]*Department of Physics, Carnegie Mellon University, 5000 Forbes Avenue, Pittsburgh, Pennsylvania 15213, USA*
[4]*Instituto de Ciencia de Materiales de Madrid CSIC, Sor Juana Inés de la Cruz 3, Campus de Cantoblanco, 28049 Madrid, Spain*

The control of magnetic interactions is becoming essential to expand/improve the applicability of magnetic nanoparticles (NPs). Here, we show that an optimized microemulsion method can be used to obtain homogenous silica coatings on even single magnetic nuclei of highly crystalline $Fe_{3-x}O_4$ NPs (7 and 16 nm) derived from a high-temperature method. We show that the thickness of this coating is controlled almost at will allowing much higher average separation among particles as compared to the oleic acid coating present on pristine NPs. Magnetic susceptibility studies show that the thickness of the silica coating allows the control of magnetic interactions. Specifically, as this effect is better displayed for the smallest particles, we show that dipole-dipole interparticle interactions can be tuned progressively for the 7 nm NPs, from almost non-interacting to strongly interacting particles at room temperature. The quantitative analysis of the magnetic properties unambiguously suggests that dipolar interactions significantly broaden the effective distribution of energy barriers by spreading the distribution of activation magnetic volumes. *Published by AIP Publishing.*
[http://dx.doi.org/10.1063/1.4974532]

I. INTRODUCTION

Key questions in nanostructured magnetic materials are how the nanostructure modifies their magnetic and electronic properties, giving rise to new phenomena taking place at the nanoscale as a result of the interaction among finite-size, surface, interfacial, and proximity effects, and how one can take advantage of those new properties to improve applications. In the particular case of magnetic iron oxide nanoparticles (NPs),[1–3] their biocompatibility has made them materials of choice for a variety of biomedical applications, such as magnetic resonance imaging (MRI), targeted drug delivery, biosensing devices, or magnetic hyperthermia.[4–8] Within these fields, a common approach to improve magnetic, optical, or chemical properties consists in the combination of magnetic NPs with other materials (nanocomposites).[9–11] Although these approaches have potential applied interest, the actual performance of the nanocomposites within the complex biological environments still makes it a challenge to bring these new nanostructures to actual diagnostic or therapeutic use. The latter is due to the fact that the physical and chemical characteristics of the particles need to be tuned to fit a series of requisites, such as optimum dispersion of the material and affinity to specific tissues or cells, trespassing physiological barriers or avoiding their rapid capture by the immune system and their rapid excretion, among others.[2,3] Besides, degradation, accumulation, and elimination of the materials introduced inside the organism are issues that still need to be fully addressed in order to use composite NPs in clinical trials in humans.[11] It is worth noting that the magnetic properties of the nanocomposites affect many of the aforementioned aspects because of the tendency of the magnetic material to agglomerate due to magnetic dipolar interactions. This may cause changes in the effective hydrodynamic radii that can drastically modify the interaction between the inoculated substances and the living organism.[2,3] Additionally, the magnetic properties of the composite can also be severely modified, which is critical regarding both its magnetic behavior and its response to external magnetic fields. In particular, the arrangement of the magnetic particles or composites in a demagnetizing configuration significantly lowers the strength of the stray magnetic fields around them. Moreover, dipolar interactions modify the energy barrier landscape affecting the magnetization reversal of the individual magnetic particles, and thus altering the relaxation and hysteretic behavior of the whole system.[12–15] The previous considerations need to be taken in mind when designing the nanostructure of the magnetic composite to actually improve the materials for *in vivo* and *in vitro* applications, mostly when restrictions in the maximum intensity of the applied magnetic fields exist.[16–20] Additionally, the processing of the magnetic material to form the composite may cause the lowering of the intrinsic particle magnetization due to its chemical degradation.[21,22] These facts could help us understand results observed in MRI or magnetic hyperthermia experiments.[16–21]

Within this framework, we have evaluated the effect of optimized silica coatings on the structural and magnetic

properties of two samples consisting primarily of highly crystalline $Fe_{3-x}O_4$ particles (7 and 16 nm) coated with oleic acid. We show that we are able to obtain homogeneous coatings and that these coatings occur on average at the single nanoparticle level. This unique control on the coating let us observe (especially for the smallest particles) how the progressive decrease in interparticle interactions leads to different magnetic regimes (from blocked to almost superparamagnetic (SPM) NPs at room temperature). Finally, we clearly show that dipolar interactions significantly broaden the effective distribution of energy barriers by spreading the distribution of activation magnetic volumes.

II. EXPERIMENTAL

A. Sample preparation

Oleic acid-coated $Fe_{3-x}O_4$ NPs were synthesized using iron(III) acetylacetonate (Sigma-Aldrich, 99%), 1-2-hexadecanediol (Sigma-Aldrich, 90%), oleic acid (Sigma-Aldrich, 90%), and benzyl-ether (Sigma-Aldrich, 98%). For the silica coating, the following reagents were used as supplied: cyclohexane (Sigma-Aldrich, 99%), polyoxyethylene(5)nonylphenyl ether (IGEPALCO-520), (3-Aminopropyl)triethoxysilane (APTES) (Sigma-Aldrich, 97%), tetraethylorthosilicate (TEOS) (Sigma-Aldrich, 99%), and NH$_4$OH 28% (w/w) -prepared in situ-. All the reactants were used in the synthesis without further purification.

1. Synthesis of oleic acid coated-$Fe_{3-x}O_4$ nanoparticles

Two samples of oleic acid-coated $Fe_{3-x}O_4$ NPs with a mean size of 7 nm and 16 nm named as **R7** and **R16**, respectively, were synthesized through the decomposition of iron(III)acetylacetonate as the metal-organic precursor and using benzyl-ether as the organic solvent, as described elsewhere.[23,24]

2. Preparation of $Fe_{3-x}O_4$@SiO$_2$ core-shell nanocomposites by a microemulsion assisted method

Silica coatings on the $Fe_{3-x}O_4$ NPs were carried out by a microemulsion method based on the base-catalyzed hydrolysis of TEOS.[25–27] Reagents were introduced by means of a pipette inside a glass test tube with screw top in the following order: 2 mmol of the surfactant IGEPAL CO-520 were dispersed in 17 ml of cyclohexane. Then, 1.6 ml of $Fe_{3-x}O_4$ NPs (10 mg·ml^{-1}), previously sonicated during one minute in an Elma Elmasonic P60H 5.75 l Heated Digital Ultrasonic Cleaner bath sonicator for 1 min, were added to the mixture. After that, 130 μl of NH$_4$OH were added. In this way, the microemulsion, consisting of an oil phase containing hydrophobic NPs and aqueous micelles containing ammonia, is formed. Finally, 150 μl of TEOS were added sequentially to the reaction mixture. After the addition of each reagent, the reaction mixture was stirred with a vortex at 2000 rpm for 1 min at room temperature to ensure the homogeneity of the mixture. The closed tube was kept under mild agitation for 72 and 96 h for the 7 and 16 nm nanoparticles, respectively. Finally, the silica-coated NPs were separated from the reaction mixture destabilizing the microemulsion with 5 ml

of methanol and allowing the particles to precipitate for 10 min, after which they were collected at the bottom of the test tube, discarding the supernatant.

The particles were washed three times in order to eliminate rests of both the surfactant and NH$_4$OH by suspending them in ethanol, centrifuging at 10 000 rpm for 30 min, and discarding the supernatant each time after centrifugation. The samples so obtained were named as R7a and R16a. In order to study the role of the silica precursor in the final properties of the magnetic composites, two modifications were undertaken to the experimental procedure mentioned earlier. For the particular case of the 7 nm-$Fe_{3-x}O_4$ NPs: (i) the amount of TEOS was reduced to 30 μl (sample name as **R7b**) and (ii) the precursor was changed to APTES (with the same 150 μl) and simultaneously the amount of NH$_4$OH was increased to 260 μl (sample name as **R7c**).

B. Experimental techniques

The particle shape and size were determined by transmission electron microscopy (TEM) performed on JEOL JEM 2000 FXII, Philips CM30, and Hitachi MT80 microscopes.

High resolution TEM (HRTEM) images were acquired with a JEOL JEM 2100 microscope. To prepare the samples for TEM experiments, one drop of a dilute suspension of NPs in the appropriate solvent was placed onto a carbon-coated copper grid and dried at room temperature. The size distributions were obtained by measuring at least 2000 particles for the oleic acid-coated samples and 500 particles for the SiO$_2$-coated samples, and the resultant histograms were fitted to log-normal functions (see Figures 1(e) and 1(f) for samples R7a and R16a, respectively, and Figures S1(b) and S1(c) in the supplementary material for R7 and R16, respectively,). The mean particle size (D_{TEM}) and the values of the standard deviation (σ) obtained from these fits are given in Table I. In order to get insight about the crystalline quality of the samples, high resolution transmission microscopy (HRTEM) carried out by using a JEOL-2100 microscope is displayed in Figures 1(a) and 1(b) for R7 and R16.

The crystallographic structure of the particles was identified by X-ray powder diffraction (XRD) performed in a PANanalytical X'Pert PRO MPD diffractometer by using Cu Kα radiation. The patterns were collected within 5° and 120° in 2θ. In all cases, the XRD spectra were indexed to an inverse spinel structure (see Figure S2, supplementary material).

The iron concentration in the samples was determined by inductively coupled plasma-optical emission spectrometry (ICP-OES) by using a Perkin Elmer OPTIMA 3200RL.

The Hydrodynamic size of the sample R7a was measured by dynamic light scattering (DLS) in a Malvern Instrument ZetaSizer Nano device.

Magnetization measurements were performed with a Superconducting Quantum Interference Device (SQUID) magnetometer. Hysteresis loops, M(H), of powder samples were recorded at 5 and 300 K under a maximum magnetic field of $\pm$50 kOe to determine the saturation magnetization M_s, which was obtained by extrapolation of the high-field region of M(H) to zero field, assuming the high-field behavior, $M(H) = M_s + \chi \cdot H$,[28] where χ is the high field susceptibility
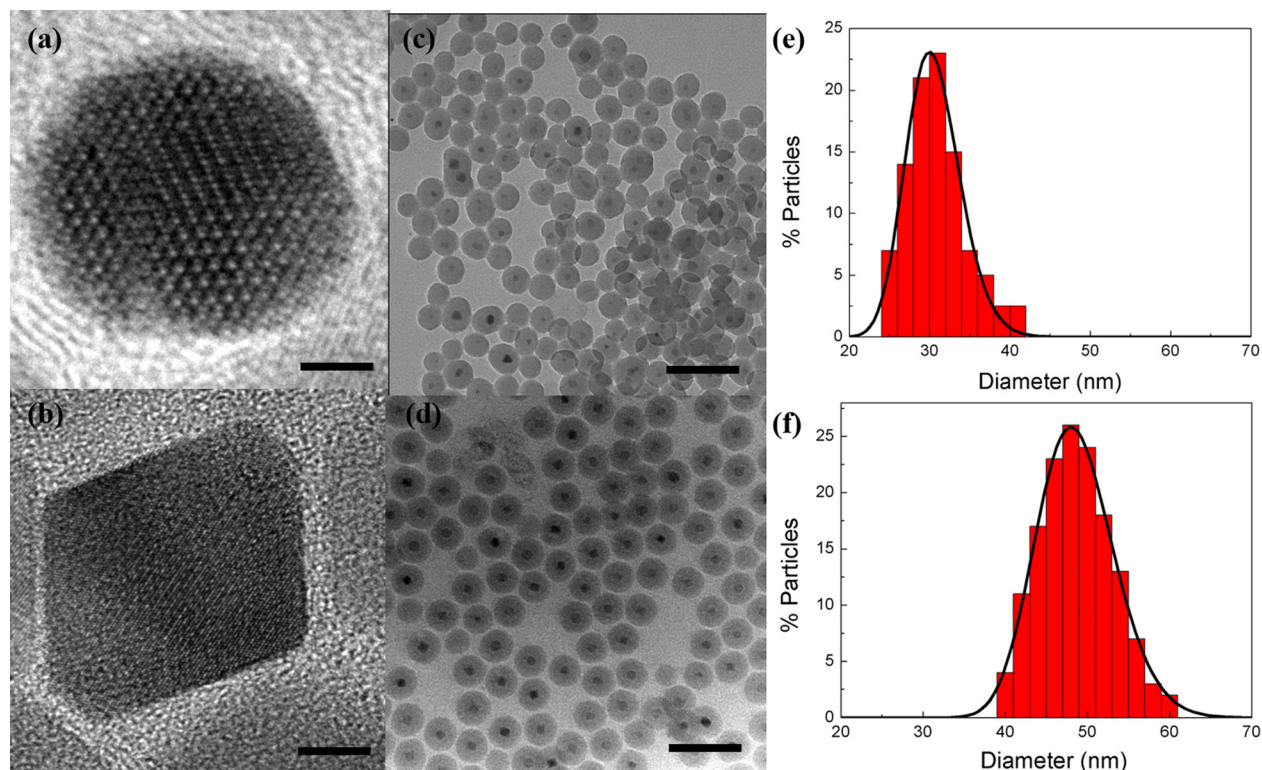
FIG. 1. HRTEM images of $Fe_{3-x}O_4$ NPs: (a) R7 and (b) R16. TEM images of Silica-coated $Fe_{3-x}O_4$ NPs: (c) R7a and (d) R16a. Particle size distribution of silica- $Fe_{3-x}O_4$ NPs: (e) R7a and (f) R16a. Scale bars: (a) 1.5 nm, (b) 4 nm, and (c) and (d) 125 nm.

that accounts for spin disorder (see Figure S4, supplementary material).[29–31] M_s values were normalized to the magnetic mass determined by ICP-OES. The thermal dependence of the low field magnetic susceptibility of colloidal suspension samples was studied after zero field cooling (M_{ZFC}) and field cooling (M_{FC}) the samples (see Figures 5 and S5, supplementary material). These curves were collected using the following protocol. The sample was cooled down from 300 to 2 K in zero magnetic field. Then, a static magnetic field of 50 Oe was applied and M_{ZFC} was measured while warming up from 2 to 300 K. Once room temperature was reached, the sample was cooled down again to 2 K while 50 Oe was applied. Finally, the sample was rewarmed up to 300 K and M_{FC} was collected under the applied field of 50 Oe.

III. STRUCTURAL CHARACTERIZATION AND REACTION MECHANISM

The TEM image of R7 shows pseudo-spherical NPs (see Figures S1(a) and S1(b), supplementary material). Analysis

of the histogram assuming a lognormal function shows D_{TEM} = 7 nm and $\sigma = 0.26$. For R16, Figures S1(c) and S1(d) show faceted NPs with $D_{TEM} = 16$ nm and $\sigma = 0.14$. Both samples show a homogeneous interparticle separation of about $d_{p-p} \sim 2$ nm, which is a clear indication of the presence of the oleic acid coating on the particle surface.[15] HRTEM images (see Figures 1(a) and 1(b) for R7 and for R16, respectively) reveal highly crystalline NPs with the absence of either sizeable defects or core-shell structure.

The mean particle diameters obtained from XRD data (D_{XRD}) were 7.0 ± 0.5 and 14.0 ± 1.0 nm for samples R7 and R16, respectively, in good agreement with the estimations from TEM (see XRD patterns for R7 and R17 in Fig. S2, supplementary material). This also confirms the high crystalline quality of the samples (absence of crystallographic domains within a single particle). As a result, these two samples can be regarded as model examples of well crystallized NPs synthesized by the organic decomposition of a metal-organic precursor $[Fe(acac)_3]$, as previously established in the literature.[10,23,28,32,33]

Figure 1(c) shows that the silica coating obtained by the optimized microemulsion method (see experimental for details) is in most of the cases observed at the single nanoparticle level. TEM sizes of 31 nm and 49 nm and average interparticle distances of 24 and 33 nm are derived from the size analysis for samples R7a and R16a, respectively. Interestingly, a direct consequence of the narrow size distribution ($\sigma < 0.2$) of the silica coatings is that extensive regions that show signatures of particle self-assembly are observed for silica coated nanoparticles (see Figure 2).

In order to gain a deeper insight into the aggregation state of the NPs, the hydrodynamic size was measured by

TABLE I. Summary of the structural and magnetic parameters of the samples.

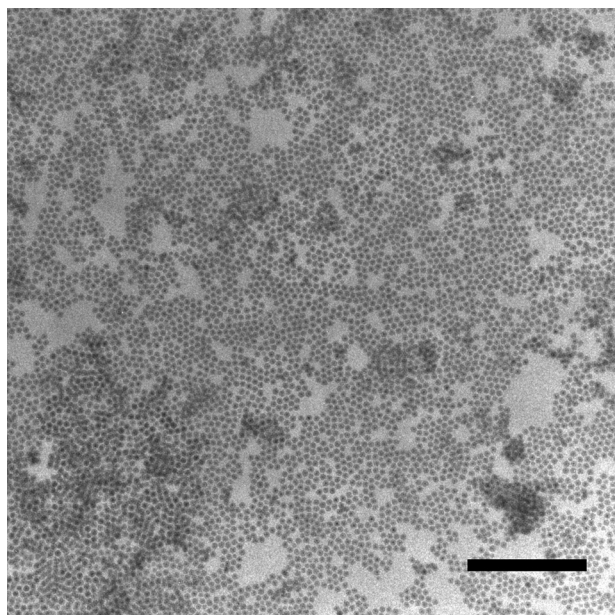| Samples	D_{TEM} (nm)	σ	T_M (K)	T_{irr} (K)
R7	7	0.26	>300	>300
R7a	31	0.12	53	170
R7b	25	0.19	59	170
R7c	7	0.26	106	220
R16	16	0.13	>300	>300
R16a	49	0.10	95	295

FIG. 2. TEM image of an ultra large self-assembly of NPs for the sample R16a. Scale bar corresponds to 1 μm.

DLS at different stages of the coating process for sample R7a (see Figure 3): (i) first, after the addition of the oleic acid-coated $Fe_{3-x}O_4$ NPs into the reaction tube and homogenization with vortex agitation, (ii) after 72 h, and (iii) after transferring the silica coated-$Fe_{3-x}O_4$ NPs to water. The initial DLS size distribution presents a peak at around 7 nm (Figure 3), which is in agreement with the size distribution of the oleic acid-coated $Fe_{3-x}O_4$ NPs obtained from TEM (Table I). After 72 h, an increase in the size was obtained, with a peak at about 37 nm that is consistent with the formation of the core-shell NPs observed in TEM. Interestingly enough, an additional increase in size was observed after transferring to water, with a peak at approximately 72 nm, indicative of particle agglomeration due to condensation
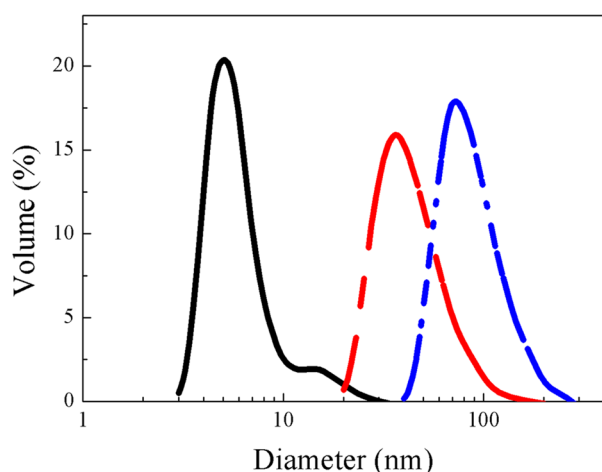

FIG. 3. Evolution of the hydrodynamic size measured with DLS of the core-shell particles for sample R7a, (i) first, after the addition of the oleic acid-coated $Fe_{3-x}O_4$ NPs into the reaction tube and homogenization with vortex agitation (solid black line), (ii) after 72 h, reaction in the microemulsion (solid red line) and after transfer*ring* the silica coated-$Fe_{3-x}O_4$ NPs to water to water (solid blue line).

reactions among the silanol groups (Si-OH) at the particles' surface. This condensation depends strongly on the polarity of the medium, being more likely in more polar solvents, as it is the case of water in comparison to ethanol.[34] This phenomenon was also confirmed by the formation of necks among several NPs in aqueous media (Figure S3, supplementary material).

It is well known that the microemulsion method shows three main advantages in comparison to other routes in solution in order to coat magnetic NPs, such as (i) more reproducibility in the results, (ii) a suitable control of the aggregation of the magnetic NPs ranging from particles of few nm of size to aggregates of about 20 nm; and (iii) a better control over the thickness of the silica shell from 20 to 100 nm.[35,36] In this method, the hydrolysis takes place at the interface between the oil phase—containing the hydrophobic phase and the silanes—and the aqueous media.[22,23] Typically, the reagents used in this method are cyclohexane as the organic medium (where the formerly oleic acid-coated NPs are dispersed), IGEPAL CO-520 as the surfactant, NH_4OH as the aqueous media, and TEOS as the silica precursor. The relative amount of aqueous components to surfactant—within the stability boundaries of the microemulsion phase diagram—determines the size and the morphology of the aqueous drops.[25,26] This enables to gain control on the kinetics of the reaction and was used to generate a variety of coatings with different aggregation states. However, there are still doubts about the reproducibility of such a method,[35,36] mainly on the role of the amount of the silica precursor or its chemical nature. In order to clarify those issues, we compared a conventional reaction (R7a; 150 μl of TEOS) with two other syntheses where we either reduced the amount (R7b; 30 μl of TEOS) or actually changed the silica precursor (R7c; 150 μl of APTES). The effects on the structural properties of the silica-coated $Fe_{3-x}O_4$ NPs were studied by electron microscopy. By largely decreasing the amount of TEOS, Figure 4(a) reveals irregular silica coatings in both size and shape for sample R7b in comparison with the standard reaction (sample R7a). TEM reveals about a 20% reduction in the mean thickness of the silica coating (from 31 to 25 nm for R7a and R7b, respectively), and a consistent, similar reduction in the surface-to-surface interparticle distance (from 24 to 19 nm for R7a and R7b, respectively), while σ evidences a considerable increase of the size dispersion. The generation of such irregular structures with a decrease of the silica thickness suggests that the shell growth was unfinished due to an insufficient amount of the silica precursor. On the other hand, when TEOS is substituted by the same amount of APTES, TEM images for sample R7c show $Fe_{3-x}O_4$ NPs without silica coating (Figure 4(b)). In addition, the low regular distance among particles (~2 to 3 nm) is indicative of the formation of a homogeneous layer of APTES molecules linked at the $Fe_{3-x}O_4$ NP surface, similar to previous works.[37,38]

IV. MAGNETIC STUDY OF THE PARTICLE AGGLOMERATION

The saturation magnetization obtained from the hysteresis loops at 5 K ($M_s = 84 \pm 2$ emu g^{-1} and 91 ± 1 emu g^{-1}
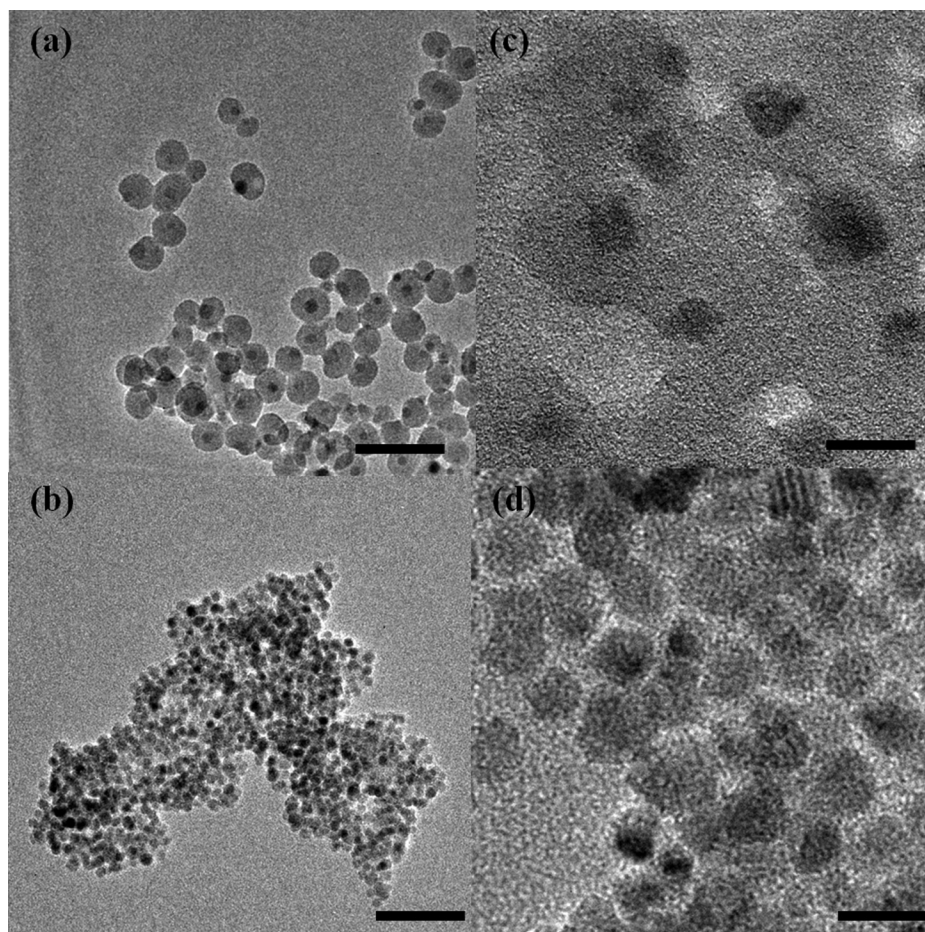
FIG. 4. TEM images for R7 with two different coatings: (a) R7b and (b) R7c. Medium-TEM resolution images: (c) R7b and (d) R7c. Scale bars: (a) and (b) correspond to 50 nm and in (c) and (d) to 10 nm.

for samples R7 and R16, respectively) were just slightly smaller than the bulk value (Figure S4, supplementary material), suggesting an almost perfect ferrimagnetic order throughout the NPs up to the surface, similar to that in some of our previous works for highly crystalline NPs.[13,15,23,28,29,32,33] It is worth noting that the additional silica coating does not alter significantly either the structure or the grade of oxidation, and therefore, the magnetization of oleic acid- coated $Fe_{3-x}O_4$ NPs.[14,15,32] Besides, recent density functional theory calculations indicate that oleic acid strongly bound to magnetite nanoparticles enhances the magnetization approximately in 1 μB per unit cell at the particle surface.[39] Consequently, although some extra oxidation of the outermost shell of the particle of about one unit cell in depth has to be considered as a result of the silica coating, no additional detrimental effects, such as freezing, canting, or disorder of the spins at the surface are expected, as suggested by the square shape of the hysteresis loops for similar samples.[14]

The size-dependent magnetic properties of nanocomposites are usually analyzed through isothermal magnetization curves, M(H), magnetic relaxation experiments, M(t), and M_{ZFC}-M_{FC} curves.[15,22,40–43] Among them, the last two methods also allow the analysis of dipolar interactions in samples with different aggregation states, since the anisotropy energy of a particle ensemble is in first approximation proportional to both the NP volume and the effective anisotropy constant. The shift to higher temperatures of the maximum of the M_{ZFC} curve with either increasing particle volume, according to

Arrhenius thermally activated processes, and/or increasing freezing phenomena due to interactions, can be decoupled in model samples.[14,15,40–44] Those combined effects have been already discussed for organic-to-inorganic coating for NPs with sizes within 5 to 20 nm.[14,15]

The M_{ZFC}-M_{FC} curves for samples R16 and R16a show two different behaviors (Fig. S5, supplementary material): oleic acid coated-NPs remain blocked even at room temperature, as expected for highly crystalline NPs with a mean size centered at 16 nm. The jump in the magnetization around T $\sim$ 120 K is attributed to the Verwey transition, which further supports the high crystalline quality and uniform stoichiometry of the sample.[45,46] In contrast, when the NPs are coated with a silica shell of about 30 nm, they follow a typical superparamagnetic behavior of a distribution of slightly interacting NPs: the M_{ZFC} curve develops a maximum around 95 K, the M_{FC} curve largely deviates from the M_{ZFC} curve below that temperature becoming flat, and both of them level off at room temperature.

On the other hand, M_{ZFC}-M_{FC} curves for samples R7, R7a, R7b, and R7c (Fig. 5) exhibit a more gradual change: Oleic acid-coated NPs evidence strong dipolar interactions since the interparticle spacing provided by the oleic acid chains is unable to obliterate the dipole-dipole magnetic interactions for highly crystalline magnetite NPs larger than about 7 nm (uppermost curve in Figure 5).

In contrast, the same magnetite NPs coated by 31 nm silica shells and with a mean interparticle separation around
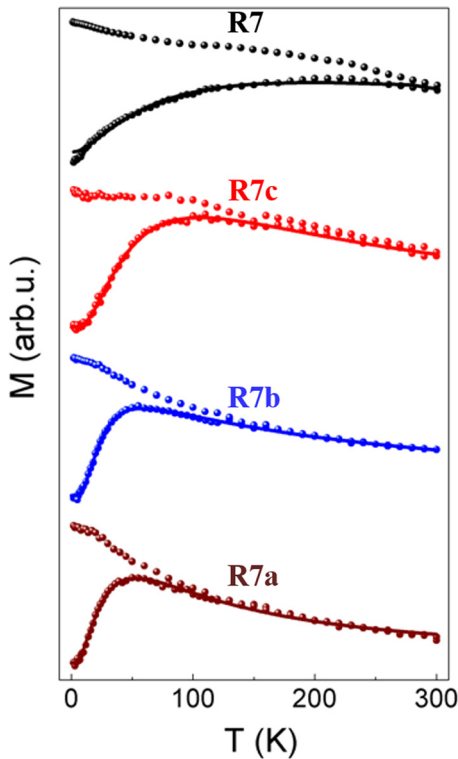
FIG. 5. ZFC-FC magnetization (H = 50 Oe) for sample R7 with different coatings: oleic acid for R7 (black spheres), APTES for R7c (red spheres), SiO_2 with a $D_{TEM} = 31$ nm (blue spheres), and SiO_2 with a $D_{TEM} = 25$ nm (brown spheres). Solid lines correspond to the fit of the ZFC curves for R7 (black line), R7c (red line), R7b (blue line), R7a (brown line) to Equation (1).

24 nm are almost non-interacting (bottom curve in Fig. 5). The sample having a slightly thinner silica shell of 25 nm and an interparticle distance of 19 nm, and the one with no thick silica coating and interparticle distance of 2–3 nm due to APTES molecules lay in between (see values of d_{p-p} for R7-R7c in Table II). Consequently, some general trends may be drawn. First, both the temperature of the maximum of the ZFC curve, ZFC-FC magnetization, and the temperature at which the ZFC and FC curves separate, T_{irr}, shift to lower temperatures as the mean distance among the magnetite cores is increased. T_M and T_{irr} for samples R7, R7a, R7b, and R7c are given in Table I. T_M decreases from the above room temperature to ca. 53 K for samples R7 and R7a, respectively, and the M_{ZFC} curve narrows while the flatness of the M_{FC} curve becomes progressively smaller below T_M.

TABLE II. Curie-Weiss temperature, T_{CW}, together with the parameters obtained from the fitting of M_{ZFC} to Equation (1), for samples R7-R7c: activation magnetic volume V_{mag}, activation magnetic diameter d_m, dimensionless standard deviation σ_v, and effective anisotropy constant K.

Samples	avg. d_{p-p} (nm)	T_{CW} (K)	V_{mag} (nm^3)	d_m[a] (nm)	σ_v[b]	K × 10^5 (erg·cm^{-3})
R7	2	…	421	9.3	1.29	3.0
R7a	24	−82	225	7.5	0.69	2.6
R7b	19	−228	227	7.6	0.81	2.6
R7c	2–3	−540	270	8.0	0.93	2.9

[a]d_m stands for activation magnetic diameter.
[b]$\sigma_v = 3 \cdot \sigma_{dm}$.

In addition, at high enough temperature, when the system becomes superparamagnetic (SPM), the low-field susceptibility follows a Curie-Weiss-like behavior, such that the inverse of the susceptibility is proportional to (T-T_{CW}) as shown in Figure S5, being T_{CW} the Curie-Weiss temperature. The linear extrapolation of the high temperature behavior intercepts the T axis at T_{CW}, which is proportional to the average strength of the dipolar interactions in the SPM state.[30] A negative value of T_{CW} indicates that the overall dipolar interactions are demagnetizing, as is commonly found in randomly oriented nanoparticulate systems.[15,30] The obtained values of T_{CW} were −82, −228, and −540 K for R7a, R7b, and R7c, respectively. Again, this result clearly indicates a decrease in the strength of the dipolar interactions when the magnetic cores are further away from each other in the nanocomposite structures.

In order to quantitatively estimate the decrease of the interparticle interaction strength by effect of the coating, we fitted the M_{ZFC}/H curves for samples R7 to R7c to the following expression, deduced from Gittleman's model[44]

$$\frac{M_{ZFC}(T)}{H} = \frac{1}{3k_BT} \int_0^{M_s V_p(T)} m^2 P(m) dm + \frac{M_s}{3K_V} \int_{M_s V_p(T)}^{\infty} m P(m) dm, \quad (1)$$

where k_B is the Boltzmann constant, K is the effective anisotropy constant, P(m) is the distribution function of the magnetizations of the effective activation volumes, and $V_p(T)$ is the activation magnetic volume at a given temperature. At any given temperature T, NPs having a volume V such that their net anisotropy energy KV is much lower than the thermal activation energy k_BT shall be in the SPM state. Bearing this in mind, the first term of Eq. (1) accounts for the contribution of SPM particles ($V < V_p(T) = \frac{25 k_B T}{K}$) and the second one corresponds to the contribution arising from the blocked particles ($V > V_p(T)$). We assumed $M_s = 84 \pm 2$ emu·g^{-1} at 5 K for all samples (Fig. S4). As a result of the fitting, K, the dimensionless standard deviation σ_v and the mean effective magnetic activation volume V_{mag} are obtained (Table II). K, σ_v, and V_{mag} progressively increase as the interparticle distance decreases. For sample R7a, where the interparticle distance is about 24 nm, the fitting yields, (i) $K = 2.6 \cdot 10^5$ erg·cm^{-3}, three times larger than the corresponding value for bulk magnetite, as expected for NPs of a few nanometers in size where the surface anisotropy is the dominant contribution,[41] (ii) $\sigma_{dm} = 0.23$, which is in good agreement with $\sigma = 0.26$ obtained from the TEM size distribution; and (iii) $V_{mag} = 225$ nm^3 that corresponds to a magnetic diameter of 7.5 nm, which is a bit larger than the TEM estimations of the mean particle size. In contrast, for the oleic acid-coated sample (R7), we obtained $K = 3.0 \cdot 10^5$ erg·cm^{-3}, $\sigma_{dm} = 0.43$, and $V_{mag} = 421$ nm^3 that corresponds to a magnetic diameter of 9.3 nm. From these results, we conclude that inter-particle interactions, which depend intrinsically on the particle distance and therefore on the type of the particle coating, slightly increase the effective anisotropy of the particles but they significantly broaden the distribution of activation

magnetic volumes, increasing the effective value of the mean magnetic diameter, and consequently, they very much broaden the distribution of effective energy barriers for magnetization reversal.[15]

V. CONCLUSION

We have demonstrated that silica coating through the microemulsion method allows homogenous coating of single magnetic nuclei that formed ultra large self-assemblies in two samples of highly crystalline $Fe_{3-x}O_4$ NPs with mean sizes of 7 and 16 nm, respectively. ZFC-FC curves reveal that silica coated-samples drastically reduce dipole-dipole interactions, which is evidenced by the narrowing of the ZFC curves, the shift to lower temperatures of the maximum of ZFC, the decrease in the mean magnetic volume and in the width of the magnetic volume distribution, and the decrease in the absolute value of negative Curie-Weiss temperature. Therefore, silica coating proves to be an advantage with respect to the former oleic acid coating, since in the latter it is difficult to keep magnetite particles larger than 10 nm in size isolated in colloidal suspension without significantly altering their magnetic properties, as they tend to agglomerate due to dipolar interactions. On the other hand, silica coating of 7 nm magnetic cores was used as a model system with tunable inter-particle distance by modifying the aggregation state through the initial conditions of the coating reaction mixture. While the departing oleic acid-coated 7 nm NPs are strongly interacting and the individually and homogeneously silica-coated NPs are almost non-interacting, it is possible to obtain a variety of intermediate aggregation states with a gradation in dipolar interaction intensity. Finally, the quantitative analysis of the magnetic properties unambiguously shows that dipolar interactions significantly broaden the effective distribution of energy barriers by broadening the distribution of activation magnetic volumes.

SUPPLEMENTARY MATERIAL

See supplementary material for particle size distribution of the oleic acid-coated samples; X-ray patterns of the samples; TEM image of Particle R7a after transfer to water; magnetization curves at 5 and 300 K for R7 and R16; M_{ZFC-FC} curves for samples R16 and R16a; Plot of the inverse of the magnetization as a function of the temperature for R7a-R7c, together with the fit of the SPM regime to a Curie-Weiss-like behavior.

ACKNOWLEDGMENTS

[1]X. Batlle and A. Labarta, J. Phys. D: Appl. Phys. **35**, R15 (2002).
[2]P. Tartaj, M. P. Morales, S. Veintemillas-verdaguer, T. González Carreño, and C. J. Serna, J. Phys. D: Appl. Phys. **36**, R182 (2003).
[3]A. G. Roca, R. Costo, A. F. Rebolledo, S. Veintemillas-Verdaguer, P. Tartaj, T. González-Carreño, M. P. Morales, and C. J. Serna, J. Phys. D: Appl. Phys. **42**, 224002 (2009).
[4]J. M. Perez, L. Josephson, T. O'Loughlin, D. Högemann, and R. Weissleder, Nat. Biotechnol. **20**, 816 (2002).
[5]Q. A. Pankhurst, J. Connolly, S. K. Jones, and J. Dobson, J. Phys. D: Appl. Phys. **36**, R167 (2003).
[6]L. Li, S. Chakrabarty, K. Spyrou, C. K. Ober, and E. P. Giannelis, Chem. Mater. **27**, 5027 (2015).
[7]P. C. Gacha, C. E. Simsa, and N. L. Allbritton, Biomaterials **31**, 8810 (2010).
[8]N. A. Jalili, M. Muscarello, and A. K. Gaharwar, Bioeng. Transl. Med. **1**, 297 (2016).
[9]J. Kim, S. Park, J. E. Lee, S. M. Jin, J. H. Lee, I. S. Lee, I. Yang, J. S. Kim, S. K. Kim, M. H. Cho *et al.*, Angew. Chem. Int. Ed. Engl. **45**, 7754 (2006).
[10]J. E. Lee, N. Lee, T. Kim, J. Kim, and T. Hyeon, Acc. Chem. Res. **44**, 893 (2011).
[11]T. Kim, E. Momin, J. Choi, K. Yuan, H. Zaidi, J. Kim, M. Park, N. Lee, M. T. McMahon, and A. Quinones-Hinojosa, J. Am. Chem. Soc. **133**, 2955 (2011).
[12]J. L. Dormann, L. Bessais, and D. Fiorani, J. Phys. C: Solid State Phys. **21**, 2015 (1988).
[13]X. Battle, N. Pérez, P. Guardia, O. Iglesias, A. Labarta, F. Bartolomé, L. M. García, J. Bartolomé, A. G. Roca, M. P. Morales *et al.*, J. Appl. Phys. **109**, 07B524 (2011).
[14]A. I. Figueroa, C. Moya, J. Bartolomé, F. Bartolomé, L. M. García, N. Pérez, A. Labarta, and X. Battle, Nanotechnology **24**, 155705 (2013).
[15]C. Moya, Ó. Iglesias, X. Batlle, and A. Labarta, J. Phys. Chem. C **119**, 24142 (2015).
[16]A. F. Rebolledo, S. Laurent, M. Calero, A. Villanueva, M. Knobel, J. F. Marco, and P. Tartaj, ACS Nano **4**, 2095 (2010).
[17]A. Beheshti, B. R. Pinzer, J. T. McDonald, M. Stampanoni, and L. Hlatky, Radiat. Res. **180**, 448 (2013).
[18]C. Martinez-Boubeta, K. Simeonidis, A. Makridis, M. Angelakeris, O. Iglesias, P. Guardia, A. Cabot, L. Yedra, S. Estradé, F. Peiró *et al.*, Sci. Rep. **3**, 1652 (2013).
[19]D. Serantes, K. Simeonidis, M. Angelakeris, O. Chubykalo-Fesenko, M. Marciello, M. P. Morales, D. Baldomir, and C. J. Martinez-Boubeta, Phys. Chem. C **118**, 5927 (2014).
[20]I. Conde-Leborán, D. Baldomir, C. Martinez-Boubeta, O. Chubykalo-Fesenko, M. P. Morales, G. Salas, J. Cabrera, D. Camarero, F. J. Teran, and D. Serantes, J. Phys. Chem. C **119**, 15698 (2015).
[21]R. Mejías, S. Pérez-Yagüe, A. G. Roca, N. Pérez, A. Villanueva, M. Cañete, S. Mañes, J. Ruiz-Cabello, M. Benito, A. Labarta, X. Battle, S. Veintemillas-Verdaguer, M. P. Morales, D. F. Barber, and C. J. Serna, Nanomedicine **5**, 397 (2010).
[22]A. G. Roca, J. F. Marco, M. P. Morales, and C. J. Serna, J. Phys. Chem. C **111**, 18577 (2007).
[23]C. Moya, X. Batlle, and A. Labarta, Phys. Chem. Chem. Phys. **17**, 27373 (2015).
[24]S. Sun and H. Zeng, J. Am. Chem. Soc. **124**, 8204 (2002).
[25]F. Arriagada and K. Osseo-Asare, J. Colloid Interface Sci. **211**, 210 (1999).
[26]K. Osseo-Asare and F. Arriagada, J. Colloid Interface Sci. **218**, 68 (1999).
[27]C. Cannas, A. Musinu, A. Ardu, F. Orrù, D. Peddis, M. Casu, R. Sanna, F. Angius, G. Diaz, and G. Piccaluga, Chem. Mater. **22**, 3353 (2010).
[28]P. Guardia, A. Labarta, and X. Battle, J. Phys. Chem. C **115**, 390 (2011).
[29]P. Guardia, B. Batlle-Brugal, A. G. Roca, O. Iglesias, M. P. Morales, C. J. Serna, A. Labarta, and X. Battle, J. Magn. Magn. Mater. **316**, e756 (2007).
[30]X. Batlle, M. García del Muro, J. Tejada, H. Pfeiffer, P. Görnert, and E. Sinn, J. Appl. Phys. **74**, 3333 (1993).
[31]X. Batlle, M. García del Muro, A. Labarta, and P. Görnert, J. Magn. Magn. Mater. **157**, 191 (1996).
[32]P. Guardia, N. Pérez, A. Labarta, and X. Batlle, Langmuir **26**, 5843 (2010).
[33]N. Pérez, F. Bartolomé, L. M. García, J. Bartolomé, M. P. Morales, C. J. Serna, A. Labarta, and X. Batlle, Appl. Phys. Lett. **94**, 093108 (2009).
[34]L. T. Zhuravlev, Colloids Surf., A **173**, 1–38 (2000).
[35]H. Yamada, C. Urata, H. Ujiie, Y. Yamauchi, and K. Kuroda, Nanoscale **5**, 6145 (2013).
[36]H. Yamada, H. Ujiie, C. Urata, E. Yamamoto, Y. Yamauchi, and K. A. Kuroda, Nanoscale **7**, 19557 (2015).
[37]R. A. Bini, R. F. C. Marques, F. J. Santos, J. A. Chaker, and M. Jafelicci, J. Magn. Magn. Mater. **324**, 534 (2012).

[38]L. Leandro, R. Malureanu, N. Rozlosnik, and A. Lavrinenko, ACS Appl. Mater. Interfaces **7**, 5797 (2015).

[39]J. Salafranca, J. Gazquez, N. Pérez, A. Labarta, S. T. Pantelides, S. J. Pennycook, X. Batlle, and M. Varela, Nano Lett. **12**, 2499 (2012).

[40]J. Vargas, W. Nunes, L. Socolovsky, M. Knobel, and D. Zanchet, Phys. Rev. B **72**, 184428 (2005).

[41]N. Pérez, P. Guardia, A. G. Roca, M. P. Morales, C. J. Serna, O. Iglesias, F. Bartolomé, L. M. García, X. Batlle, and A. Labarta, Nanotechnology **19**, 475704 (2008).

[42]B. D. Cullity and C. D. Graham, *Introduction to Magnetic Materials* (John Wiley & Sons, 2011).

[43]A. G. Roca, D. Carmona, N. Miguel-Sancho, O. Bomatí-Miguel, F. Balas, C. Piquer, and J. Santamaría, Nanotechnology **23**, 155603 (2012).

[44]J. Gittleman, B. Abeles, and S. Bozowski, Phys. Rev. B **9**, 3891 (1974).

[45]E. J. W. Verwey, Nature **144**, 327 (1939).

[46]A. Kuipers and V. Brabers, Phys. Rev. B **14**, 1401 (1976).